Magnetic transitions and spin dynamics in the $3d^1$ system K_2NaCrO_8 investigated by magnetization and ^{23}Na NMR

K.-Y. Choi
Department of Physics, Chung-Ang University, 221 Huksuk-Dong, Dongjak-Gu, Seoul 156-756, Republic of Korea

S. Nellutla, A. P. Reyes, P. L. Kuhns, Y.-J Jo, and L. Balicas
National High Magnetic Field Laboratory, Tallahassee, Florida 32310, USA

H. Nojiri
Institute for Materials Research, Tohoku University, Katahira 2-1-1, Sendai 980-8577, Japan

M. Pati and N. S. Dalal
Department of Chemistry and Biochemistry, Florida State University, Tallahassee, Florida 32306, USA
and National High Magnetic Field Laboratory, Tallahassee, Florida 32310, USA
(Received 15 September 2008; published 15 December 2008)

We report pulsed magnetization and ^{23}Na NMR studies of a quantum phase transition and its associated spin dynamics in a $3d^1$ system, using the alkali-metal peroxychromate K_2NaCrO_8. This is an example of a Cr^{5+}-based $S=1/2$ and $I\sim 0$ material with a clearly defined $T_N=1.7$ K in zero applied field (H). Its magnetization (M) shows a nonlinear increase with H, in contrast to a simple three-dimensional antiferromagnet, and saturates at $H_C=7.4$ T. This easily accessible H_C allows for a detailed study by ^{23}Na NMR of the magnetic-field-induced quantum phase transition from the antiferromagnetically ordered to a ferromagnetically polarized phase. The critical exponent of $M(T)\sim(1-T/T_N)^{\beta}$ is 0.44 ± 0.05 at $H=5$ T but shows a definitive increase to 0.53 ± 0.05 at 6.8 T, close to H_C. This suggests that while the magnetic behavior of K_2NaCrO_8 is largely describable by a mean-field theory, the field dependence of β remains unexplained.

DOI: 10.1103/PhysRevB.78.214419 PACS number(s): 76.60.−k, 75.30.Kz, 75.60.Ej, 75.30.Cr

I. INTRODUCTION

A large experimental and theoretical effort has been devoted to the investigations of magnetism based on spin-1/2 transition-metal oxides due to pronounced quantum effects.[1] Among inorganic materials, copper-, vanadium-, and titanium-based oxides with one hole ($Cu^{2+};3d^9$) or one electron ($V^{4+};3d^1$) and ($Ti^{3+};3d^1$) in the d shell often realize structurally well-defined spin-1/2 systems. In these compounds the on-site Coulomb interaction is larger than the width of the energy band. Thus, spin dynamics is often closely related to charge, orbital, and lattice degrees of freedom. On the one hand, this leads to exotic ground states and low-energy excitations. On the other hand, this puts an obstacle in understanding spin dynamics of a simple spin-1/2 system.[2,3]

Noticeably, the electronic structure of the Cr ion in the rare oxidation state of 5+ ($3d^1;S=1/2;90.5\%$ $I=0$) makes it one of the simplest magnetic systems. Chromium oxide (CrO_3) in highly basic aqueous media reacts with hydrogen peroxide (H_2O_2) to yield salts known as alkali-metal peroxychromates M_3CrO_8 ($M=Na^+$, K^+, Rb^+, and Cs^+).[4–6] These alkali-metal peroxychromates provide a route to achieve an $S=1/2$ quantum spin system.

It is noteworthy that the Cr (5+) ion here is bonded to four peroxide $(O_2)^{2-}$ ions rather than eight oxide $(O)^{2-}$ ions. Much of the peroxide ion $(O_2)^{2-}$ is derived from the reactant hydrogen peroxide (H_2O_2), as discussed in the comprehensive review article by Dickman and Pope.[5] The most direct evidence for its presence comes from the x-ray diffraction studies of single crystals. The crystal structure of M_3CrO_8 shows that the four $(O_2)^{2-}$ ions are covalently bonded to the central Cr^{5+} ion forming a $[Cr(O_2)_4]^{3-}$ unit with dodecahedral geometry. Both oxygen atoms of $(O_2)^{2-}$ are bonded to the Cr ion, albeit one of the O's is slightly closer (1.89 Å) to the Cr ion than the other O ion (1.94 Å). The CrO_8^{3-} ion can thus be thought of as a chromate ion (CrO_4^{2-}), in which the $(O)^{2-}$ ions are replaced by $(O_2)^{2-}$ ions. The structure is held together by these CrO_8^{3-} anions and three monovalent alkali-metal cations that balance the charge in a three-dimensional orthorhombic lattice, as illustrated in Fig. 1(a). Since the alkali-metal cations and the $(O_2)^{2-}$ are all diamagnetic, the magnetism in the lattice originates essentially from the Cr^{5+} ion.[5–8] It is possible that the anisotropic structure and the plausible reorientational motion of the $(O_2)^{2-}$ ions could play a role in the structural changes and hence the magnetism of the parent lattice at low temperatures. Low-temperature x-ray and neutron-diffraction studies are needed to investigate this aspect.

Among the peroxychromate family, K_2NaCrO_8 is chosen for a detailed study due to its ease of growing good single crystals. Its ground state is given by the metal-based d_{z^2} orbital and has a well-characterized antiferromagnetic (AF) state at accessible temperature of $T_N\sim 1.7$ K in zero field (*vide infra*).[8] K_2NaCrO_8 has an orthorhombic crystal structure (space group *Pbcm*) with the lattice parameters $a=8.6031$ Å, $b=7.9792$ Å, and $c=9.2520$ Å [see Fig. 1(a)]. In order to figure out a spin topology we considered all possible exchange paths including the combined shortest Na/K···O distance and the largest O···Na/K···O angles,

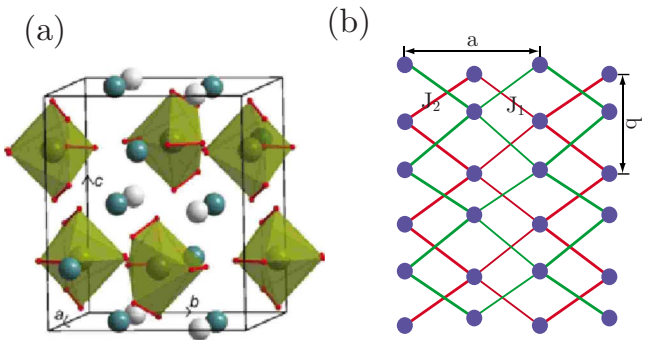

FIG. 1. (Color online) (a) Unit cell of the K_2NaCrO_8. Color code is as follows: Blue (K), gray (Na), dark yellow (Cr), and red (O). The dodecahedral arrangement of the peroxyligands around Cr ions is shown by the polyhedra. (b) Distorted square lattice formed in *ab* plane. The blue ball represents the Cr^{5+} ions. The thick and thin lines denote two different exchange interactions J_1 and J_2, respectively.

leading to the strongest antiferromagnetic interactions.

The Cr^{5+} ions along the *a* axis are separated by 8.588 Å and interact via the exchange path Cr–O···K···O–Cr with two different K···O distances of 2.781 and 3.045 Å. Along the *b* axis there exist two different kinds of zigzag chains with Cr···Cr distances 5.837 and 5.888 Å mediated by the exchange paths Cr–O···Na···O–Cr (Na···O distances: 2.426 and 2.363 Å) and Cr–O···K···O–Cr (K···O distances: 2.860 and 3.128 Å), respectively. If only the shortest distances between Cr ions are taken into account, the spins in the *ab* plane consist of two independent distorted square lattices, which are shifted along the *b* axis with respect to each other [see Fig. 1(b)]. Along the *c* axis, Cr ions interact via alternating zigzag chains with Cr···Cr distances 6.289 and 6.336 Å. The exchange paths involved are Cr–O···Na···O–Cr (Na···O distances: 2.363 and 2.426 Å for the Cr···Cr distance of 6.289 Å) and Cr–O···K···O–Cr (Na···O distances: 2.626 and 2.926 Å for the Cr···Cr distance of 6.336 Å). These chains are perpendicular to the *ab* plane. Here, the O···K···O angle is 161° and the O···Na···O angle is 94°. In addition, Cr^{5+} ions along a diagonal direction of the unit cell are exchange coupled by Cr–O···K(Na)···O–Cr with O···K(Na) distance of 2.354 (2.626) Å with alternating Cr···Cr distances of 5.974 and 6.243 Å, respectively. We note that the latter two spin chains penetrate the distorted square lattices without forming a three-dimensional (3D) spin network. Thus, at zeroth level approximation, K_2NaCrO_8 might be considered as a quasi-two-dimensional spin system.

In this study, we report the magnetization and ^{23}Na NMR measurements of the mixed alkali-metal peroxychromate K_2NaCrO_8 as a function of temperature and external field. The field dependence of magnetization shows the saturation of magnetization at $H_C=7.4$ T. NMR measurements provide microscopic information on spin dynamics in a crossover regime between antiferromagnetically ordered and ferromagnetically polarized phases.

II. EXPERIMENTAL DETAILS

Single crystals of K_2NaCrO_8 were prepared by modification of the method of Riesenfeld.[4] The synthesis involves the reduction of Cr(VI) by 30% H_2O_2 at 5 °C in the 1:1 molar mixture of aqueous NaOH and KOH. *dc* static susceptibility was measured on the single crystals in the temperature range of 1.8–300 K using a superconducting quantum interference device (SQUID) magnetometer [Quantum Design magnetic properties measurement system (MPMS)]. Magnetization measurements were carried out by means of a standard inductive method using compensated pickup coils and a nondestructive pulse magnet. Fast pulsed magnetic fields up to 10^3 T/s were generated by a capacitor bank of 90 kJ.[9] The sample was immersed in liquid ^3He to reach temperature as low as 0.4 K. Specific-heat measurements on single crystals were performed by means of a Quantum Design physical properties measurement system (PPMS) using the relaxation technique over a temperature range of 0.34–8 K. ^{23}Na NMR spectra and spin-lattice relaxation rate $1/T_1$ of single crystals were obtained using a locally developed NMR spectrometer equipped with a ^3He cryostat and a high homogeneity 17 T sweepable magnet. The resonance spectrum was obtained by sweeping the frequency at a fixed magnetic field. $1/T_1$ was obtained by measuring the recovery of the spin-echo intensity as a function of time after saturation of the ^{23}Na spins.

III. RESULTS AND DISCUSSION

A. EPR of K_2NaCrO_8 and related lattices

Understanding the nature of the Cr^{5+} unpaired electron is important in understanding antiferromagnetic interactions present in the M_3CrO_8 family. Electron paramagnetic resonance (EPR) is therefore the tool of choice as it provides fundamental information about the spin ground state. From ambient to liquid-helium temperatures, the polycrystalline EPR spectra of M_3CrO_8 are characteristic of a spin $S=1/2$ system with no hyperfine interactions.[6–8,10] The *g* value is close to the free-electron *g* of 2, indicating that the orbital angular momentum is largely quenched by the crystal-field effects. In particular, the EPR spectra of K_2NaCrO_8 at frequencies as high as 360 GHz were reported by Cage *et al.*[10] The basic parameters obtained were the three principal *g* values: $g_{xx}=1.9636$, $g_{yy}=1.9696$, and $g_{zz}=1.9851$. The fact that $g_{zz}>g_{xx},g_{yy}$ implies that the unpaired electron occupies the metal's d_{z^2} atomic orbital. The *g* values were slightly temperature dependent down to about 6 K, the lowest temperature employed. Further measurements at lower temperatures, especially around and below the phase-transition temperature of 1.7 K (*vide infra*) are planned in the near future, when a Dewar leading to temperatures below 1.7 K would become available.

B. Static susceptibility, specific heat, and magnetization

Figure 2 shows the temperature dependence of the magnetic susceptibility, $\chi(T)$ $(=M/H)$ of K_2NaCrO_8 measured in an applied field of 0.2 T. $\chi(T)$ exhibits a broad maximum around 2.39 K, indicative of development of short-range magnetic interactions. The bulk susceptibility data above 7 K are analyzed using the Curie-Weiss law,

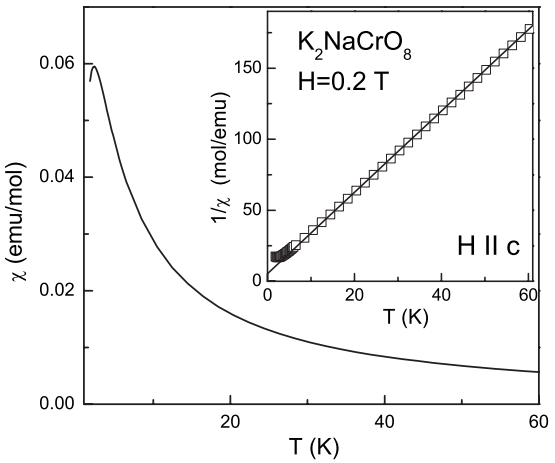

FIG. 2. Temperature dependence of static susceptibility in an applied field of $H=0.2$ T for $H\|c$ axis. The open squares in the inset represent the temperature dependence of the inverse susceptibility. The solid line is a fit to the Curie-Weiss law. See the text for details.

$$\chi_{\mathrm{CW}}(T) = \chi_0 + \frac{C_{\mathrm{mol}}}{(T-\Theta)}. \tag{1}$$

The first term χ_0 is the temperature-independent contribution arising from the diamagnetism of the core electron shells and the Van Vleck paramagnetism of the open shells of the Cr^{5+} ions. The second term is the Curie-Weiss contribution. Here C_{mol} is the molar Curie constant and Θ is the Curie-Weiss temperature. A fit to the Curie-Weiss law is shown in the inset, which yields C_{mol} as 0.384 mol^{-1} K and Θ as −2.54 K. The negative value of Θ indicates dominant antiferromagnetic interactions between Cr^{5+} ions. The effective magnetic moment is thus given by $\mu_{\mathrm{eff}}=\sqrt{3k_BC_{\mathrm{mol}}/N\mu_B^2}=1.75\mu_B$, which is close to the spin only value of $g\sqrt{S(S+1)}\mu_B=1.71\mu_B$ for Cr^{5+} with a g factor of $g=1.9851$.[8] The almost perfect quenching of orbital moments is consistent with the rather weak spin-orbit coupling in this system.

Preliminary specific-heat measurements show a λ-like anomaly at $T_N\sim 1.7$ K, indicating a transition to a long-range magnetic ordering (see Fig. 3). Since the Curie-Weiss

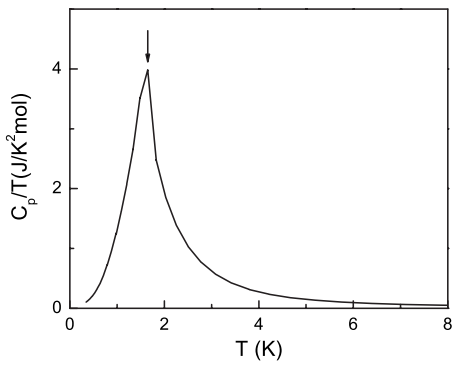

FIG. 3. Specific heat of K_2NaCrO_8 between 0.4 and 8 K in zero applied magnetic field. The arrow indicates the Néel temperature, $T_N=1.7$ K.

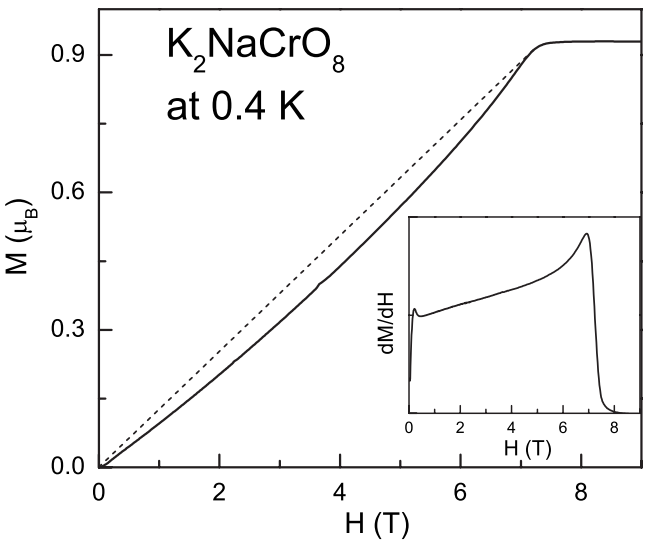

FIG. 4. Field dependence of magnetization at 0.4 K measured using a pulsed magnet. The inset shows the derivative of the magnetization with respect to the applied field. A nonlinear increase in magnetization is observed.

temperature $|\Theta|=2.54$ K and $T_N\sim 1.7$ K have the same order of magnitude, the magnetic behavior is largely described by a mean-field theory. This suggests that the spin network is more complicated than a quasi-two-dimensional lattice, which is conjectured from the exchange paths of the shortest separation of the Cr ions. By using the relation $\Theta=-\Sigma_i z_i J_i S(S+1)/3k_B$, we can relate the Curie-Weiss constant to the sum of the exchange parameters J_i to the ith neighboring Cr moment. From the experimental value of $|\Theta|=2.54$ K, one obtains $\Sigma_i z_i J_i=10.16$ K. Using $z_i=8$ the exchange parameter J_i is estimated to be 1.27 K. This is consistent with earlier works.[6–8]

Figure 4 shows the magnetization behavior in external fields of up to 10 T at 0.4 K. The magnetization curve exhibits a nonlinear increase contrary to linear field dependence expected for conventional antiferromagnets. The antiferromagnetic state undergoes a transition to the field-induced ferromagnetic phase at $H_C=7.4$ T. The saturation field H_C is identified as a peak of field derivative of the magnetization, dM/dH (see the inset of Fig. 4). The continuously increasing convex magnetization is not due to a spin-flop transition. Further, it is not ascribed to a field-induced change of a magnetic structure because the NMR spectrum does not show any additional splitting in an external field (see below). Also, it cannot be ascribed to spin anisotropy since the orbital angular momentum is largely quenched by crystal-field effects (see below). Rather, it might be associated with the fact that magnetization is suppressed by residual low-dimensional spin fluctuations.

C. ^{23}Na NMR

To investigate the spin dynamics of the Cr^{5+} electronic spins, we probed the ^{23}Na nuclei ($I=3/2$) which are coupled to the Cr^{5+} magnetic ions via dipole-dipole interactions. The NMR spectra were obtained by monitoring the fast Fourier

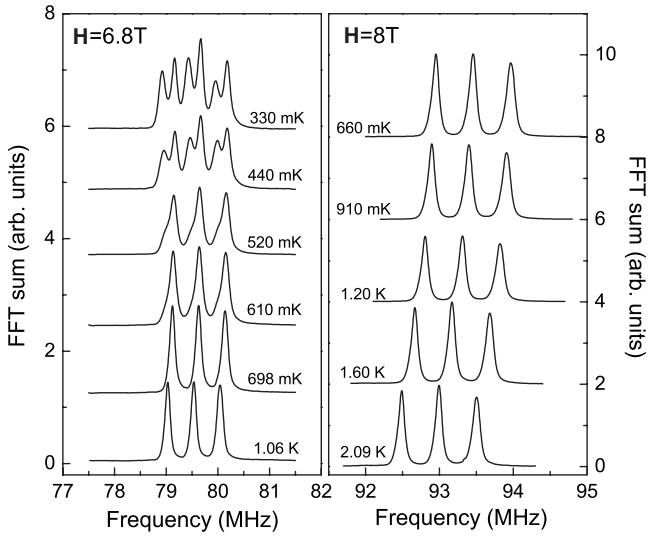

FIG. 5. ^{23}Na NMR spectra of a single crystal of K_2NaCrO_8 obtained by monitoring the FFT sum of a spin echo as a function of temperature at two fixed fields $H=6.8$ T (below the saturation field) and $H=8$ T (above the saturation field), respectively.

transform (FFT) sum of a spin echo as a function of the irradiation frequency at a fixed magnetic field. Typical examples of ^{23}Na NMR spectra at $H=6.8$ T (below H_C) and $H=8$ T (above H_C) are shown in Fig. 5. At 6.8 T and 1.06 K three spectral lines are observed as expected from the coupling of an electron with the ^{23}Na $I=3/2$ nuclei in a paramagnetic system. We find no hint for a field-induced structural change. The central peak corresponds to the $1/2 \leftrightarrow -1/2$ transition while the satellite peaks to the $\pm 3/2 \leftrightarrow \pm 1/2$ transitions. At 6.8 T, upon cooling below 1.06 K, each peak splits and thus at the lowest measured temperature (330 mK) six distinct overlapped peaks are observed. This indicates the development of a Néel-type long-range ordering. The separation between the main peaks and their shoulders increases slightly with decreasing temperature and the relative intensities of the shoulders become stronger with decreasing temperature. On the other hand, at $H=8$ T, only three peaks are observed even at the very low temperature while the NMR lines strongly shift to higher frequency as temperature approaches zero. This is consistent with the evolution of a spin-polarized ferromagnetic (FM) state.

In Fig. 6 we plot the temperature dependence of the relative NMR shift with respect to the unshifted frequency $f_0 = \gamma H_0$

$$K(\%) = \frac{f_{\text{peak}} - f_0}{f_0} \times 100. \tag{2}$$

Here, γ is the gyromagnetic ratio of the ^{23}Na nuclei and f_{peak} is the frequency of the central line in a magnetic field of $H=5$, 7.45, and 10.21 T, respectively. At 5 T $K(T)$ increases with decreasing temperature and then shows a peak at about 1.2 K. This is correlated with the transition to the Néel ordered state from a paramagnetic one. This is shown more clearly in the semilogarithmic plot in the inset of Fig. 6. In

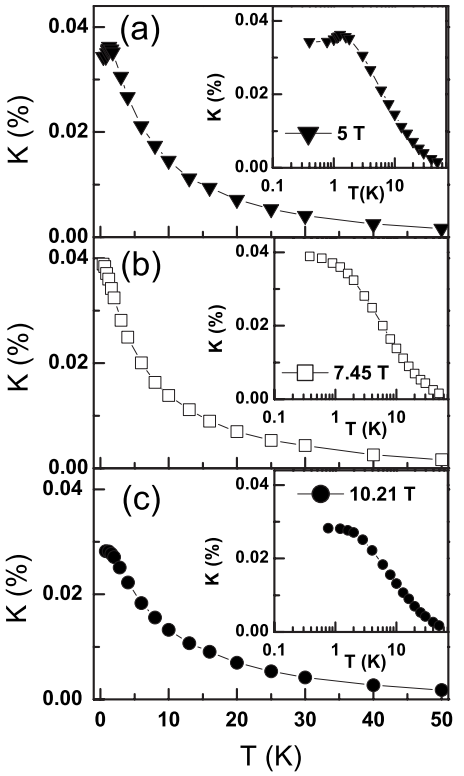

FIG. 6. ^{23}Na shift K versus temperature at an external field (a) 5, (b) 7.45, and (c) 10.21 T, respectively. The inset displays the respective K versus T on a logarithmic temperature scale for a clearer presentation of the low-temperature behavior.

proximity to the saturation field, $K(T)$ continues to increase without any obvious saturation. In the spin-polarized ferromagnetic state ($H=10.21$ T), $K(T)$ seems to show a tendency to saturate in the sub-Kelvin region.

Figure 7 displays the K versus $\chi(T)$, the electronic susceptibility for $H=5$ T above T_N. The temperature dependence of K is fitted to the equation

$$K = K_0 + \left(\frac{A}{N_A \mu_B}\right)\chi(T), \tag{3}$$

where K_0 is the orbital shift, A is the ^{23}Na hyperfine coupling constant, and N_A is the Avogadro number. Here the zero in-

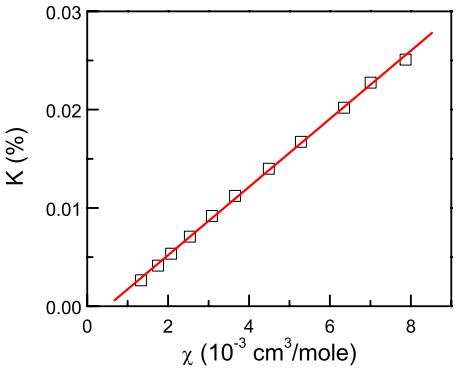

FIG. 7. (Color online) Relative frequency shift of the central NMR line as a function of dc susceptibility, $\chi(T)$ for $H=5$ T above T_N. The solid line is the linear fit to the data according to Eq. (3).

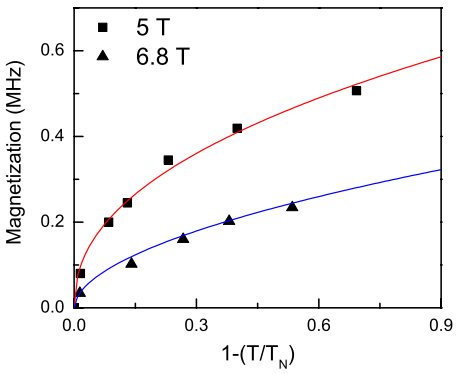

FIG. 8. (Color online) Temperature dependence of the splitting at an external field of 5 and 6.8 T. The solid curve is a fit to the scaling function $M(T) \sim (1-T/T_N)^{\beta}$, yielding $\beta=0.44$ at $H=5$ T to $\beta=0.53$ at $H=6.8$ T. The average value of 0.50 ± 0.05 is indicative of a 3D quantum phase transition.

tercept gives the orbital shift. The shift data fit nicely in the temperature range 4–50 K, yielding the hyperfine coupling constant $A=0.0346$ T/μ_B. This value will be used in discussing the ^{23}Na nuclear spin-lattice relaxation rate, $1/T_1$ (*vide infra*).

Figure 8 shows the temperature dependence of the peak separation ΔM, which is defined as the frequency difference between the two split peaks of the central line in Fig. 5. This is proportional to the magnitude of the staggered magnetization. Thus, the dependence of ΔM on temperature follows a critical behavior corresponding to a second-order transition connected with a continuous change of the staggered magnetization. This is described by the scaling function $M(T) \sim (1-T/T_N)^{\beta}$, where β is a critical exponent. As the magnetic field increases from $H=5$ T to 6.8 T, the transverse magnetic moments are reduced while the longitudinal magnetic moments become more and more polarized. This is reflected in the reduction in the magnitude of the peak separation with increasing field. The critical exponent changes from $\beta=0.44 \pm 0.005$ at $H=5$ T to $\beta=0.53 \pm 0.005$ at $H=6.8$ T. This is close to a mean-field value of $\beta=0.5$ for a 3D quantum phase transition, suggesting that the spin dynamics of the studied system is largely governed by 3D interactions although there is some indication of a low dimensionality of spin correlations (see Fig. 4). The changing critical exponent might be associated to the effect of magnetoelastic coupling while approaching a quantum critical point. In order to pin down the exact origin, a detailed magnetocaloric study is needed.

In order to probe the low-energy spin excitations, we investigated the ^{23}Na nuclear spin-lattice relaxation rate $1/T_1$ in the temperature range 0.33–50 K at 5, 6.8, 7.45, 8, and 10.21 T. $1/T_1$ is measured by monitoring the recovery of the ^{23}Na nuclear magnetization after the application of a $\pi/2$ rf pulse. The central line was selectively irradiated. The recovery curve of the longitudinal magnetization is fitted by a double exponential function, $M(T)=M_{\infty}[1-(0.1e^{-t/T_1}+0.9e^{-t/6T_1})]$, characteristic of the central transition of $I=3/2$ nuclei. In Fig. 9, we summarize the temperature dependence of the spin-lattice relaxation rate. A peak in $1/T_1$ at 1.29 K and 0.58 K for the $H=5$ and 6.8 T, respectively,

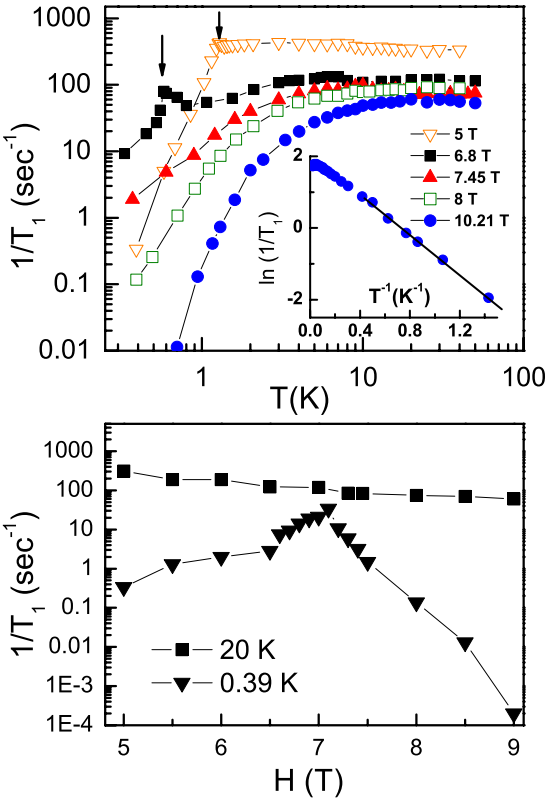

FIG. 9. (Color online) (Upper panel) ^{23}Na spin-lattice relaxation rate $1/T_1$ on a logarithmic temperature scale at various magnetic field of 5, 6.8, 7.45, 8, and 10.21 T, respectively. The arrows indicate the transition to an antiferromagnetically ordered state. The inset shows $\ln(1/T_1)$ as a function of inverse temperature at $H=10.21$ T. The solid line is a fit to the function $1/T_1=C\exp(-\Delta/T)$, yielding the spin gap Δ of 5.6 K. (Lower panel) Field dependence of ^{23}Na spin-lattice relaxation rate $1/T_1$ on a logarithmic scale at 20 and 0.39 K, respectively.

reflects the phase transition from the paramagnetic state to the antiferromagnetically ordered state. Above $T_N=1.29$ K at 5 T, $1/T_1$ is largely temperature independent. On changing the field from 5 to 10.21 T, $1/T_1$ decreases continuously, consistent with the increased stiffness of spins. This feature is typical for a spin-lattice relaxation process driven by the spin-flips of the Cr^{5+} paramagnetic moments. For a short correlation time τ, namely, $\omega\tau \ll 1$, $1/T_1$ is approximated as[11]

$$T_1^{-1} \approx \frac{2}{5}\gamma^2 A^2 S(S+1)\tau, \tag{4}$$

where γ is the gyromagnetic ratio of the ^{23}Na nuclei, A is the hyperfine coupling, and S is the spin of the electronic magnetic moments. With $\gamma=7.0746\times10^7$ s^{-1} T^{-1}, $A=0.0346$ T, and $1/T_1=310$ s^{-1}, the correlation time of the Cr^{5+} spins is estimated to be $\tau=2.29\times10^{-10}$ s for $H=5$ T. As the field increases from 5 T to 11 T, the correlation time (τ) is gradually shortened to 3.37×10^{-11} s. At very low temperatures, as the field increases, $1/T_1$ decreases by several orders of magnitude with decreasing temperature, indicating the formation of a spin gap in the spectrum of magnon excitations

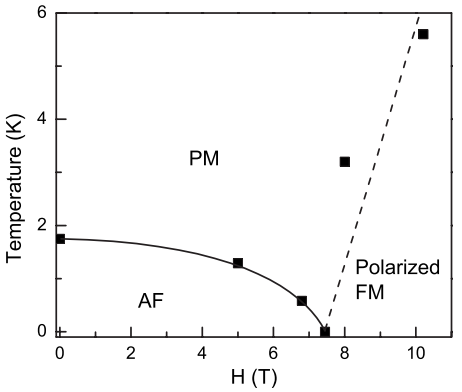

FIG. 10. T versus H phase diagram as determined from the ^{23}Na NMR measurements. PM, AF, and polarized FM stand for paramagnetic, antiferromagnetic, and polarized ferromagnetic phase, respectively. The solid and dashed lines are a guide for a phase boundary.

in the ferromagnetically polarized state. Ferromagnetic spin waves show a field-dependent gap given by

$$\Delta_{\mathrm{FP}} = g\mu_B(H - H_C). \tag{5}$$

With $g=1.9851$ and $H_C=7.4$ T, we obtain $\Delta_{\mathrm{FP}}=3.8$ K at $H=10.21$ T. The gap in the magnon spectrum can be also extracted from the temperature dependence of $1/T_1 = C\exp(-\Delta/T)$ with $\Delta=5.6$ K. This value is larger than the estimated one from the saturation field. Possible reasons for the difference between them are magnetoelastic coupling and anisotropic exchange interactions, which lead to a deviation from the linear field dependence of the gap. In this case, the gap extracted from the saturation field becomes less reliable.

Finally, we present the phase diagram in Fig. 10 as a function of a magnetic field. The AF ordering temperature is identified by the sharp peak in $1/T_1$. The spin gap in the polarized FM phase is estimated from the activation behavior of $1/T_1$.

IV. CONCLUSIONS

To conclude, we have presented the combined magnetization, the specific heat, and the ^{23}Na NMR measurements of the mixed alkali-metal peroxychromate K_2NaCrO_8, which is an example of a Cr^{5+}-based $S=1/2$ and $I\sim 0$ antiferromagnet. At zero field, this system undergoes a transition to the Néel ordered state at $T_N\sim 1.7$ K. The magnetization shows that the quantum phase transition occurs at $H_C=7.4$ T from the antiferromagnetically ordered to ferromagnetically polarized state. ^{23}Na NMR measurements enable us to extract the critical exponent $\beta=0.44\pm0.005$ (0.53 ± 0.005) of $M(T) \sim (1-T/T_N)^{\beta}$ for $H=5$ (6.8) T as well as to determine the magnetic phase diagram. Although the magnetic behavior of K_2NaCrO_8 could be largely described by a mean-field model, there are minor anomalies in the temperature and field dependence of magnetization and the magnitude of spin gap in the polarized FM state, which call for a deeper theoretical analysis of this system. Finally, we note that this study opens up an avenue of research since K_2NaCrO_8 is just the forerunner of this family of Cr^{5+}-based $3d^1$ systems, which all might be interesting to follow up.[12–14]

ACKNOWLEDGMENTS

Much of the experimental work was carried out at NHMFL. We thank the State of Florida and the NSF Cooperative Agreements No. DMR 0654118, No. DMR 0520481, and No. DMR 0506946.

[1] P. Lemmens, G. Güntherodt, and C. Gros, Phys. Rep. **375**, 1 (2003).
[2] Y. H. Shing and D. Walsh, Phys. Rev. Lett. **33**, 1067 (1974).
[3] A. Syamal, Coord. Chem. Rev. **16**, 309 (1975).
[4] E. H. Riesenfeld, Chem. Ber. **38**, 4068 (1905).
[5] M. H. Dickman and M. T. Pope, Chem. Rev. (Washington, D.C.) **94**, 569 (1994).
[6] N. S. Dalal, J. M. Millar, M. S. Jagadeesh, and M. S. Seehra, J. Chem. Phys. **74**, 1916 (1981).
[7] S. Nellutla, K.-Y. Choi, M. Pati, J. van Tol, I. Chiorescu, and N. S. Dalal, Phys Rev. Lett. **99**, 137601 (2007).
[8] B. Cage and N. S. Dalal, Chem. Mater. **13**, 880 (2001).
[9] H. Nojiri, K.-Y. Choi, and N. Kitamura, J. Magn. Magn. Mater. **310**, 1468 (2007).
[10] B. Cage, A. K. Hassan, L. Pardi, J. Krzystek, L. C. Brunel, and N. S. Dalal, J. Magn. Reson. **124**, 495 (1997).
[11] A. Abragam, *Principles of Magnetic Resonance* (Oxford Science Publications, Oxford, 1960).
[12] B. Cage, W. Geyer, K. A. Abboud, and N. S. Dalal, Chem. Mater. **13**, 871 (2001).
[13] A. Harter, B. Cage, P. Nguyen, K. A. Abboud, and N. S. Dalal, Polyhedron **24**, 2264 (2005).
[14] S. Nellutla, G. W. Morley, J. van Tol, M. Pati, and N. S. Dalal, Phys. Rev. B **78**, 054426 (2008).